A numerical investigation of sub-wavelength resonances in polygonal metamaterial cylinders

Arslanagic, Samel; Breinbjerg, Olav

Published in:
Optics Express

Link to article, DOI:
10.1364/OE.17.016059

Publication date:
2009

Document Version
Publisher's PDF, also known as Version of record

A numerical investigation of sub-wavelength resonances in polygonal metamaterial cylinders

Samel Arslanagić* and Olav Breinbjerg

Department of Electrical Engineering, Electromagnetics Systems Group,
Technical University of Denmark,
DK-2800 Kgs. Lyngby, Denmark
**sar@elektro.dtu.dk*

Abstract: The sub-wavelength resonances, known to exist in metamaterial radiators and scatterers of circular cylindrical shape, are investigated with the aim of determining if these resonances also exist for polygonal cylinders and, if so, how they are affected by the shape of the polygon. To this end, a set of polygonal cylinders excited by a nearby electric line current is analyzed numerically and it is shown, through detailed analysis of the near-field distribution and radiation resistance, that these polygonal cylinders do indeed support sub-wavelength resonances similar to those of the circular cylinders. The dispersion and loss, inevitably present in realistic metamaterials, are modeled by the Drude and Lorentz dispersion models to study the bandwidth properties of the resonances.

OCIS codes: (160.3918) Metamaterials; (290.5850) Scattering, particles.

References and links

1. G. V. Eleftheriades, and K. G. Balmain, eds., *Negative-refraction metamaterials – fundamental principles and applications* (John Wiley & Sons, 2005).
2. C. Caloz, and T. Itoh, eds., *Electromagnetic metamaterials – Transmission Line Theory and Microwave Applications* (John Wiley & Sons, 2006).
3. N. Engheta, and R. W. Ziolkowski, eds., *Metamaterials – physics and engineering explorations* (John Wiley & Sons, 2006).
4. N. Engheta, and R. W. Ziolkowski, "A positive future for double negative materials," IEEE Trans. Microw. Theory Tech. **53**(4), 1535–1556 (2005).
5. A. Alù, and N. Engheta, "Resonances in sub-wavelength cylindrical structures made of pairs of double-negative and double-positive or epsilon-negative and mu-negative coaxial shells," *in Proceedings of the International Electromagnetics and Advanced Applications Conference*, (Turin, Italy, 2003), pp. 435–438.
6. A. Alù, and N. Engheta, "Polarizabilities and effective parameters for collections of spherical nanoparticles formed by pairs of concentric double-negative, single-negative, and/or double-positive metamaterial layers," J. Appl. Phys. **97**(9), 094310 (2005).
7. R. W. Ziolkowski, and A. Erentok, "Metamaterial-based efficient electrically small antennas," IEEE Trans. Antenn. Propag. **54**(7), 2113–2130 (2006).
8. H. Stuart, and A. Pidwerbetsky, "Electrically small antenna elements using negative permittivity resonators," IEEE Trans. Antenn. Propag. **54**(6), 1644–1653 (2006).
9. S. Arslanagić, R. W. Ziolkowski, and O. Breinbjerg, "Analytical and numerical investigation of the radiation from concentric metamaterial spheres excited by an electric Hertzian dipole," Radio Sci. **42**(6), RS6S16 (2007).
10. S. Arslanagić, R. W. Ziolkowski, and O. Breinbjerg, "Analytical and numerical investigation of the radiation and scattering from concentric metamaterial cylinders excited by an electric line source," Radio Sci. **42**(6), RS6S15 (2007).
11. H. Wallén, H. Kettunen, and A. Sihvola, "Electrostatic resonances of negative-permittivity interfaces, spheres, and wedges," *in Proceedings of The First Intl. Congress on Advanced Electromagnetic Materials for Microwave and Optics*, (Rome, Italy, 2007).
12. H.-Y. She, L.-W. Li, O. J. F. Martin, and J. R. Mosig, "Surface polaritons of small coated cylinders illuminated by normal incident TM and TE plane waves," Opt. Express **16**(2), 1007–1019 (2008).
13. S. Arslanagić, N. C. J. Clausen, R. R. Pedersen, and O. Breinbjerg, "Properties of sub-wavelength resonances in metamaterial cylinders," *in Proceedings of NATO Advanced Research Workshop: Metamaterials for Secure Information and Communication Technologies*, (Marrakesh, Morocco, 2008).
14. S. Arslanagić, and O. Breinbjerg, "Sub-wavelength resonances in polygonal metamaterial cylinders," *in Proceedings of IEEE AP-S USNC/URSI National Radio Science Meeting*, (San Diego, USA, 2008).
15. ANSOFT, Version 10.1.3, Copyright (C), 1984–2006 Ansoft Corporation.
16. C. A. Balanis, *Advanced Engineering Electromagnetics* (John Wiley & Sons, 1989).

#113924 - $15.00 USD Received 6 Jul 2009; revised 20 Aug 2009; accepted 21 Aug 2009; published 26 Aug 2009

17. It should be noted that the initial HFSS model utilized radiation boundaries instead of the perfectly matched layers. However, such a model resulted in inconsistent results, in particular with varying side length w, despite the fact that the distance from the perfectly matched layers to the polygonal cylinders and the ELC was larger than $\lambda_0 / 4$ as suggested by HFSS, and despite improved discretization along the radiation boundaries. This problem was alleviated by use of perfectly matched layers for which the default discretization options were sufficient to obtain consistent and convergent results.
18. It is important to note that the delta energy, ΔE, which is the difference in the relative energy error from one adaptive solution to the next, and serves as a stopping criterion for the solution, was set to 0.01 in all cases. This value of ΔE was targeted and obtained in 3 consecutive adaptive solutions for the 48-, 24-, 12-, and 8-sided PCs, and in 2 consecutive adaptive solutions for the 4-sided PCs.
19. For the 4-sided PC, the MNG shell in the non-dispersive model is described by permeability $\mu_2 = -4\mu_0$ and a loss tangent of 0.001 for all frequencies.

1. Introduction

The past decade has witnessed an enormous activity in the research of a new class of materials, commonly referred to as metamaterials (MTMs), which are typically synthesized by distributing inclusions, each contained inside a unit cell, of various shapes and properties into a host medium, see *e.g.*, [1–4] and the extensive list of works referenced therein. Very important examples of these materials are double-negative (DNG) materials, characterized by a negative real part of the permittivity and permeability, as well as single-negative (SNG) materials such as epsilon-negative (ENG) materials, which posses a negative real part of the permittivity, and mu-negative (MNG) materials, which possess a negative real part of the permeability. The primary goal of numerous investigations has been the clarification of the fundamental physical properties of these novel materials, as well as their potential applications [1–4].

Specifically, the potential of DNG and/or SNG materials, as well as combinations of these with normal double-positive (DPS) materials, characterized by a positive real part of the permittivity and permeability, for sub-wavelength waveguides, cavities, scatterers, and radiators of different canonical shapes was demonstrated [3–14]. For cylindrical geometries it was shown [10] that a set of MTM concentric circular cylinders excited by a nearby electric line current (ELC) possesses sub-wavelength resonances where the excitation of specific modes leads to *e.g.*, large radiated power for constant ELC.

The purpose of this work is to investigate how the sub-wavelength resonances in MTM cylinders are affected by the shape of the cylinder cross section; in particular, its deviation from the perfect circular shape. From a theoretical point of view such an investigation helps determining the relationship between the shape, on one side, and properties, on the other side, of the material structure. From the practical point of view, an exact circular shape of the MTM structure might be difficult to manufacture due to the shape of the individual unit cells and inclusions forming the MTM. Other geometries might be fitted more accurately by the individual cells of the MTM, and thus it is important to investigate the influence of the deviation of the cylindrical surface on the sub-wavelength resonances. In the present work a set of MTM concentric polygonal cylinders excited by a nearby ELC is analyzed numerically and it is shown that the polygonal cylinders do possess sub-wavelength resonances similar to those of the circular cylinders. The analysis is performed by means of the ANSOFT High Frequency Structural Simulator (HFSS) [15] and includes investigations of the near-field distribution as well as the radiation resistance in the case of simple, but lossy and dispersive, MTMs. This work constitutes an extension of [14] with a full account of the modeling process for the HFSS analysis and additional polygonal configurations.

The manuscript is organized as follows. In Section 2, the investigated configurations are defined and the analysis techniques described. Section 3 presents the numerical results for lossless as well as lossy and dispersive MTM structures. The variation of the radiation resistance with the geometry and the location of the ELC is studied, and the observed sub-wavelength resonances are further confirmed through analysis of the near-field distributions. The results are summarized and conclusions are drawn in Section 4. Throughout the

#113924 - $15.00 USD Received 6 Jul 2009; revised 20 Aug 2009; accepted 21 Aug 2009; published 26 Aug 2009

manuscript, the time factor $\exp(j\omega t)$, with ω being the angular frequency and t being the time, is assumed and suppressed.

2. Configuration and theoretical background

2.1 Configuration

The cross-sections of the circular and polygonal cylinder configurations are shown in Fig. 1. In Fig. 1(a), a core circular cylinder (region 1) of radius ρ_1 is covered by a concentric circular shell (region 2) of outer radius ρ_2. In Fig. 1(b), a core regular polygonal cylinder (region 1), with n sides and a circumscribed circle of radius ρ_1, is covered by a concentric regular polygonal shell (region 2) with n sides and a circumscribed circle of radius ρ_2. Although Fig. 1(b) shows just the n = 8-sided polygonal cylinders, this work also investigates 48-, 24-, 12-, and 4-sided polygonal cylinders. Other non-circular configurations could obviously have been employed in the analysis; however, these polygonal cylinder configurations have been selected since they provide a gradual degradation of the perfect circular cylinder.

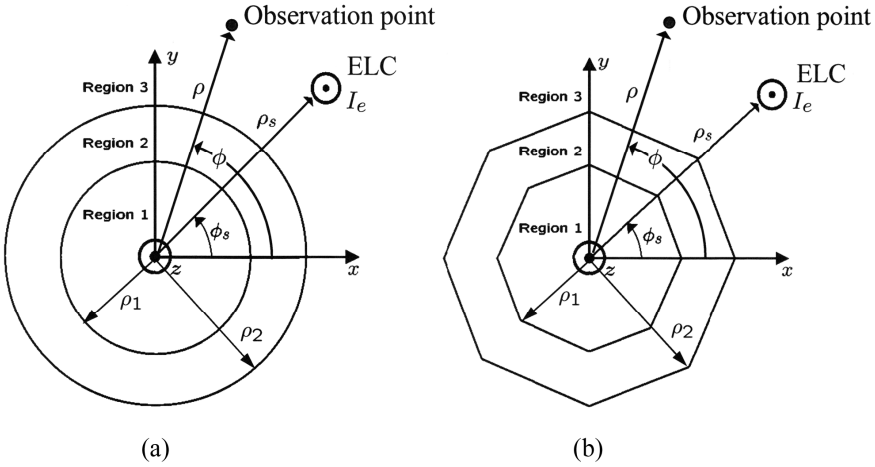

Fig. 1. The cross-section of the circular (a) and polygonal (b) configurations.

For both configurations, regions 1 and 2 are surrounded by free space (region 3) with the permittivity ε_0 and permeability μ_0, and thus the wave number $k_0 = \omega\sqrt{\varepsilon_0\mu_0}$ and intrinsic impedance $\eta_0 = \sqrt{\mu_0/\varepsilon_0}$. Moreover, regions 1 and 2 are composed of simple, lossy, and dispersive DPS, DNG, or SNG materials with a permittivity, $\varepsilon_i = \varepsilon_i' - j\varepsilon_i''$, and a permeability, $\mu_i = \mu_i' - j\mu_i''$, ($i = 1$ (2) for region 1 (2)). The cylinders are illuminated by an infinite ELC with the constant current I_e that is parallel to the cylinders and can be located in any of the three regions. The cylindrical (ρ, ϕ, z) - coordinate system and the Cartesian (x, y, z) - coordinate system are introduced with the z - axis coinciding with the common axis of the cylinders. The coordinates of the observation point are (ρ, ϕ) while those of the ELC are (ρ_s, ϕ_s). In what follows the configuration of the circular cylinders is referred to as the CC configuration, whereas the configuration of the polygonal cylinders is referred to as the PC configuration.

#113924 - $15.00 USD Received 6 Jul 2009; revised 20 Aug 2009; accepted 21 Aug 2009; published 26 Aug 2009

2.2 Methods of analysis

For the CC configuration, see Fig. 1(a), an exact solution is established using the well-known eigenfunction expansion technique, see *e.g*., [16, Ch. 11]. Below, only the main points of this solution procedure are included while the details and the full analytical solution can be found in [10].

The incident field of the ELC is first expanded in terms of cylindrical wave functions. Then, the unknown fields in the three regions, *i.e*., the scattered field in the region containing the ELC and the total fields in the remaining regions, are likewise expanded in terms of cylindrical wave functions. The expansions of the incident and unknown fields represent multipole expansions of the fields. The unknown fields contain a set of unknown expansion coefficients: $C_{1n}, C_{2n}, C_{3n},$ and C_{4n} (C_{1n} is the expansion coefficient for region 1, C_{2n} and C_{3n} are those for region 2, and C_{4n} is that for region 3), where n designates the mode number in the multipole expansion, *i.e*., $n = 0$ is the monopolar mode, $n = 1$ is the dipolar mode and so on. These unknown coefficients depend on the location of the ELC and are readily determined by enforcing the boundary conditions at the interfaces between the three regions. Upon the determination of the unknown fields, a number of quantities may be derived as was done in [10]; please refer also to Section 2.3 below for specific derived quantities which are of relevance to the present work.

For the PC configuration, see Fig. 1(b), a numerical solution is established using the ANSOFT HFSS software [15]. To this end, a finite length current tube with radius *a*, current I_e, and axis at (ρ_s, ϕ_s) , modeling the ELC, and the finite length MTM polygonal cylinders are positioned between, and perpendicular to, two parallel, perfectly electrically conducting infinite plates with separation *h*. By image theory [16, Ch. 7], these plates model the infinite MTM cylinder and ELC. Between the perfectly conducting plates, uniform perfect matching layers which model free-space radiation, have thickness *d*, circumscribe a square of side length *w*, and have their corners and edges joined, are inserted. A graphical illustration of the HFSS model of the PC configuration is presented in Fig. 2, where an 8-sided PC configuration is shown, clearly illustrating the details of the employed model. Additional details as well as the values of specific parameters for the HFSS model of the PC structures are given in Section 3.

2.3 Derived quantities and resonance condition

For the CC configuration, significant attention was devoted in [10] to the amount of the total power, P_r^t , radiated by the ELC near-by the circular cylinders

$$P_r^t = \left(\frac{1}{4}\eta_0 I_e^2\right)\left[\frac{k_0}{4}\sum_{n=0}^{N_{\max}} \tau_n^2 (3-\tau_n) \mid \alpha_n \mid^2\right], \tag{1}$$

for a given constant value of the current I_e along the ELC, relative to the power, P_r^i , radiated by the ELC having the same I_e and being situated alone in free space

$$P_r^i = \left(\frac{1}{4}\eta_0 I_e^2\right)\left[\frac{k_0}{2}\right]. \tag{2}$$

In (1), the quantity $\alpha_n = J_n(k_0\rho_s) + C_{4n}$ when the ELC is in region 3, while $\alpha_n = C_{4n}$ when the ELC is in any other region. The function $J_n(\cdot)$ is the Bessel function of order *n*.The symbol τ_n is the Neumann number, *i.e*., $\tau_n = 1$ for $n = 0$, and $\tau_n = 2$ otherwise, while $N_{\max}$ is the truncation limit which is chosen to ensure convergence of the cylindrical wave expansions.

#113924 - $15.00 USD Received 6 Jul 2009; revised 20 Aug 2009; accepted 21 Aug 2009; published 26 Aug 2009

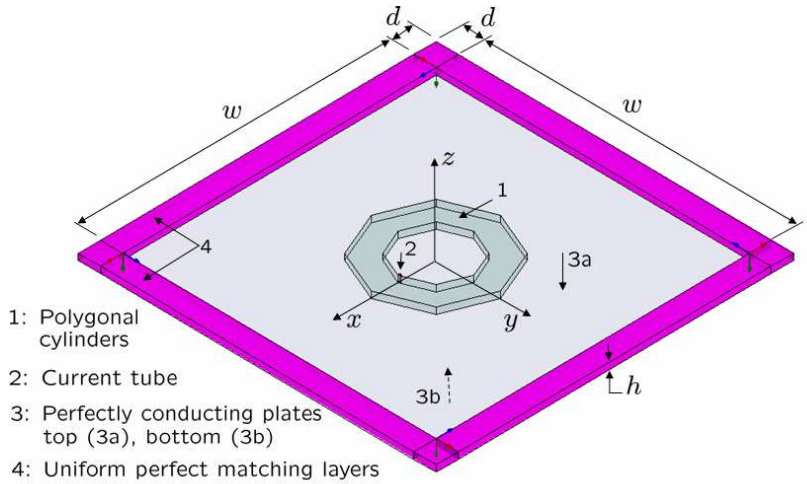

Fig. 2. The HFSS model of the PC configuration. In the shown case, the PC configuration consists of an 8-sided polygonal cylinder structure. The figure is not to scale.

Since the total power P_r^t is proportional to $|C_{4n}|^2$, it is clear that large values of P_r^t will occur if the amplitude of the expansion coefficients C_{4n} becomes large. For electrically small, *i.e.*, sub-wavelength structures, these coefficients become large and thus exhibit a resonance when the approximate condition

$$\frac{\rho_1}{\rho_2} \approx \sqrt[2n]{\frac{(\mu_2+\mu_1)(\mu_2+\mu_0)}{(\mu_2-\mu_1)(\mu_2-\mu_0)}}\,, \qquad (n \geq 1) \qquad (3)$$

is satisfied [3,4,10]. It was shown in [3,4,10] that in order to satisfy (3), at least one of the parameters, μ_1 or μ_2, needs to be negative, *i.e.*, DNG and/or MNG materials must be incorporated to obtain a resonant sub-wavelength structure. It is noted that these sub-wavelength resonances are due to the presence of specific natural modes in the structure [10]. An intuitive explanation for the occurrence of the sub-wavelength resonances is [3,4] that the DNG and /or MNG region acts a tuning element providing the opposite reactance of the DPS region as seen by the ELC, and a condition of zero reactance is thus facilitated by the combination of the two regions.

It is clear that possible resonances can be revealed from observations of quantities such as the radiated power (1). However, large values of P_r^t also occur if the current I_e is increased; a scenario which obviously does not correspond to the excitation of sub-wavelength resonances in the structure. In consequence hereof, the so-called total radiation resistance, R_r^t, which is the radiation resistance of the ELC radiating near-by the circular cylinders, defined by

$$R_r^t = \frac{2P_r^t}{I_e^2}\,, \qquad (4)$$

with P_r^t given by (1), will be considered in the present work . Clearly, the quantity in (4) is independent of the current I_e, and thus, significantly large values of R_r^t can be related directly to the excitation of sub-wavelength resonances inside the structure. In similitude, the radiation resistance of the ELC situated alone in free space, denoted by R_r^i, is defined by

#113924 - $15.00 USD Received 6 Jul 2009; revised 20 Aug 2009; accepted 21 Aug 2009; published 26 Aug 2009

$$R_r^i = \frac{2P_r^i}{I_e^2} \ , \tag{5}$$

with P_r^i given by (2).

3. Numerical results

3.1 Initial remarks

According to Section 2.3 and [10], a dipole ($n=1$) mode resonance, leading *e.g.*, to large values of radiated power (and by reciprocity also scattering cross-section), occurs for the CC configuration if region 1 is free space, region 2 is a MNG material with $(\varepsilon_2, \mu_2) = (1\varepsilon_0, -4\mu_0)$, and $(\rho_1, \rho_2) = (6,\ 10.0329)$ mm. It is next investigated if a similar resonance occurs for the PC configuration.

Both CC and PC configurations have the same radius ρ_1, current $I_e = 1$ A, and the same material parameters in all of the forthcoming calculations. Thus, the structures to be examined are either a circular or an *n*-sided polygonal MNG shell excited by a nearby ELC. The frequency of operation is $f_0 = 300$ MHz with free-space wavelength $\lambda_0 = 1$ m. For the PC configuration, the ELC is modeled by a perfectly conducting current tube of radius $a = 0.15\ \text{mm} \approx \lambda_0 / 6666$, while the side length of the square circumscribed by the uniform perfect matching layers is $w = 600\ \text{mm} \approx \lambda_0 / 1.6$, and the plate separation is set to $h = 1\ \text{mm} = \lambda_0 / 1000$. The thickness of the perfectly matching layers is set to $d = 12.25\ \text{mm} \approx \lambda_0 / 81$, which is the default value suggested by HFSS for the chosen size of w.

As to the HFSS model, the following important remarks are in order. First, with the HFSS model described above [17] the model of the ELC was tested by comparing the calculated radiation resistance in free space with the known analytical result. With the current along the current tube set to $I_e = 1$A, the radiation resistance calculated by HFSS was found to be $R_r^i = 0.57\ \Omega/\text{mm}$. This result compares very well with the exact value of an infinitely long ELC of the same radius, for which $R_r^i = 0.59\ \Omega/\text{mm}$ [13], and thus verifies the established HFSS model of the ELC. Second, the sharp corners of the 4-sided PC result in numerical instability - even for finer discretization of the mesh and after addition of losses in the MNG shell. To avoid this problem, the sharp corners were rounded to a bend radius ρ_f and moreover, an imaginary component was added to the permeability such that $\mu_2 = (-4 - j0.004)\mu_0$, resulting in a magnetic loss tangent of 0.001. In order to investigate the effect of the bend radius on the sub-wavelength resonances of the 4-sided PC, two bend radii are considered: $\rho_{f1} = 1/\sqrt{2}$ mm and $\rho_{f2} = \rho_{f1}/2 = 1/(2\sqrt{2})$. For the first (second) bend radius, the configuration is referred to as the 4-sided(1) PC (4-sided(2) PC). It was verified that the rounding of the sharp corners in the 4-sided polygonal cylinder structure and the inclusion of magnetic loss resulted in consistent results which were discretization independent [18].

3.2 Radiation resistance

Figure 3 shows the radiation resistance $R_r^t\left[\Omega/\text{mm}\right]$ as a function of the outer radius ρ_2 for the 48-, 24-, 12-, 8-, and 4-sided PC configuration when the ELC is located in region 1 at $(\rho_s, \phi_s) = (5.75\ \text{mm}, 0^o)$. The results for the reference CC configuration are also included.

#113924 - $15.00 USD Received 6 Jul 2009; revised 20 Aug 2009; accepted 21 Aug 2009; published 26 Aug 2009

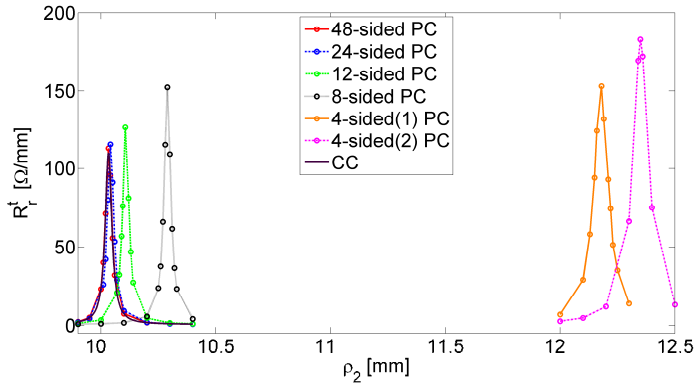

Fig. 3. Radiation resistance R_r^t [Ω / mm] as a function of the outer radius ρ_2 for the circular (CC) and *n*-sided polygonal cylinder configurations (PCs), with *n* = 48, 24, 12, 8, and 4. For the 4-sided PC, the 4-sided(1) PC has the bend radius of the corner rounding $\rho_{f1} = 1/\sqrt{2}$ mm, whereas the 4-sided(2) PC has $\rho_{f2} = \rho_{f1}/2 = 1/(2\sqrt{2})$ mm. In all cases, the ELC is located in region 1 at $(\rho_s, \phi_s) = (5.75 \text{ mm}, 0^o)$.

It is interesting to observe that the resonance occurs also for the PCs though at a different value of ρ_2 depending on the number of sides n. For large n, *i.e.*, for $n = 48$ and $n = 24$, the outer radius ρ_2 at resonance, and the radiation resistance R_r^t, is very close to that of the CC. This can be understood in view of the large number of polygon sides. As n decreases, and the PCs thus deviates considerably from the CC, the outer radius ρ_2 at resonance increases slightly for the 12- and 8-sided PCs while the radiation resistance R_r^t increases more notably. These effects are even more pronounced with the two 4-sided PCs for which both the outer radius ρ_2 at resonance as well as the radiation resistance R_r^t increases. The values of the outer shell radius ρ_2 at resonance and the associated values of the radiation resistance R_r^t are summarized in Table 1. For comparison, it is recalled that the ELC in free space has $R_r^i = 0.59\,\Omega/$ mm. For the chosen ELC location, it is not only clear to observe that the results for the two 4-sided PCs, although qualitatively the same, differ quantitatively from those of the remaining structures, but also that they differ quantitatively between each other. The reason for the quantitative difference between the results for the two 4-sided PCs is given in Section 3.3.

#113924 - $15.00 USD Received 6 Jul 2009; revised 20 Aug 2009; accepted 21 Aug 2009; published 26 Aug 2009

Table 1. The outer radius, ρ_2, and radiation resistance, R_r^t, of the resonant CC and PCs. In all cases, the ELC is located in region 1 at (ρ_s, ϕ_s) = (5.75 mm, 0^o).

Configuration	ρ_2 [mm]	R_r^t [Ω / mm]
CC	10.0329	110.2
48-sided PC	10.033	113.2
24-sided PC	10.041	115.8
12-sided PC	10.106	126.8
8-sided PC	10.289	152.4
4-sided(1) PC	12.18	153.3
4-sided(2) PC	12.35	182.9

Figure 4 shows the radiation resistance R_r^t as a function of the location of the ELC along the *x*-axis, *i.e.*, for $(\rho_s, \phi_s = 0^o)$, in region 1 for the resonant CC and PC configurations.

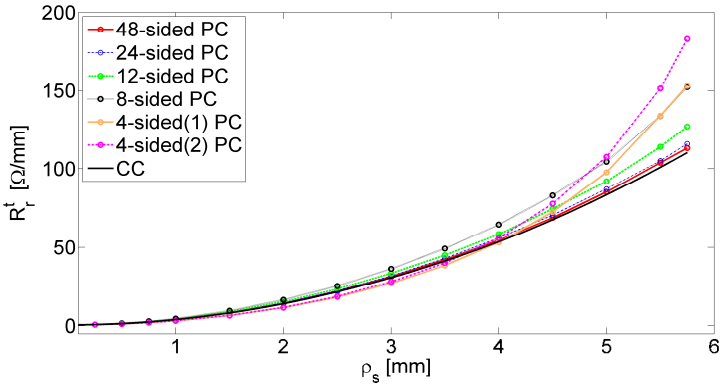

Fig. 4. Radiation resistance R_r^t [Ω / mm] as a function of the ELC location $(\rho_s, \phi_s = 0^o)$ for the circular (CCs) and *n*-sided polygonal configurations (PCs), with *n* = 48, 24, 12, 8, and 4. For the 4-sided PC, the 4-sided(1) PC has the bend radius of the corner rounding $\rho_{f1} = 1/\sqrt{2}$ mm, whereas the 4-sided(2) PC has $\rho_{f2} = \rho_{f1}/2 = 1/(2\sqrt{2})$.

In all cases, the radiation resistance increases monotonically as the ELC approaches the respective MNG shells. Moreover, the quantitative behaviour of the radiation resistance is rather similar for all configurations for $\rho_s \le 4$ mm, though differences occur as the ELC approaches the MNG shell; this is particularly the case with the 8-sided and the two 4-sided PC configurations for which significantly larger values of the radiation resistance are obtained when the ELC is close to the MNG shell. Since the difference between R_r^t for the circular and polygonal configurations is significant only for ρ_s close to ρ_1, and the qualitative behaviour of the radiation resistance for the investigated ELC locations is the same for all configurations, it is concluded that the shape of the cylindrical structure is not of primary

#113924 - $15.00 USD Received 6 Jul 2009; revised 20 Aug 2009; accepted 21 Aug 2009; published 26 Aug 2009

importance for the existence of sub-wavelength resonances, although different values may be obtained with different structures for specific ELC locations. Thus, results similar to those with the circular configuration can also be obtained with the polygonal ones.

3.3 Near-field distribution

In the following, the above findings related to the sub-wavelength resonances are further illustrated and explained with an analysis of the electric near-field distributions. For all of the following near-field plots, the magnitude of the total electric near field is plotted in the xy-plane, and in all cases, the linear dynamic range is set to [150-170000] V/m.

As regards the initial examination of the near-field properties of the CC and PC configurations, the ELC is located in region 1 at $(\rho_s, \phi_s) =$ (5.75 mm, 0°); see also Figs. 5(a) and (b) for a graphical indication of the ELC location in the respective cases. The respective magnitudes of the electric near field are depicted in Figs. 5 (c)-(h) for the resonant CC configuration and 48-, 24-, 12-, 8-, and 4-sided (1) PC configurations.

In all cases, a dipolar mode is observed, clearly demonstrating that the resonances shown in Figs. 3 and 4 are due to the excitation of this resonant mode in CC and PC configurations. It is interesting to note that the fields of the PC configurations attain higher values than the fields of the CC configuration. Moreover, the fields of the PCs become more confined near the corners of the structure as the number of sides decreases; once again, this effect is particularly in strong evidence for the 4-sided PC. As to the 4-sided PC configuration, the following additional remarks are in order. As was shown in Fig. 3, the results for the two 4-sided PC configurations, although qualitatively the same, differ quantitatively from the remaining structures for the particular ELC location investigated therein. Moreover, they also differ quantitatively from each other for the particular ELC location, although the change in the bend radius from the 4-sided PC(1) to 4-sided PC(2), is not very large. The reason for the latter is straightforward to grasp by observing *e.g.*, Fig. 5(h). Obviously, for the specific ELC location near-by the inner right corner of the 4-sided PC(1) structure, the field attains very high values in the region around the inner right and left corners of the 4-sided PC(1) configuration. Although not shown inhere, as the bend radius decreases, the field values in the said regions increases. As (some of) the rounded corners in the 4-sided PC configurations are located in the region of the high field values, see Fig. 5(h), and as the structures are electrically small, even small changes of the bend radius may lead to different values of the resonances (since the field amplitudes may thus change drastically) as well as different outer radii at which the resonance is attained for the 4-sided PC configuration. This explains the quantitative difference observed between the two 4-sided PCs for the ELC located near-by a corner of these structures.

It is important to note that the sub-wavelength resonances of the PCs are not restricted to locations of the ELC near the corners of the structure. In the following, the location of the ELC is varied along a straight line starting at the point $(\rho_s, \phi_s) =$ (5.75 mm, 0°) and extending along a path located near-by, parallel to and equal in length to a face of the 8-sided PC. More specifically, the ELC is at a point corresponding to 1/8, 1/4, and 1/2 of the length of this path, as measured from its starting point. For a graphical indication of the ELC location in the respective cases see Fig. 6(a), [in which $(\rho_s, \phi_s) =$ (5.55 mm, 5.625°)], Fig. 6(b) [in which $(\rho_s, \phi_s) =$ (5.32 mm,11.25°),], and 6(c), [in which (ρ_s, ϕ_s) = (5.29 mm,22.5°)]. While the latter location of the ELC is symmetric with respect to a plane of the structure, the former two are not. The magnitudes of the electric field corresponding to the ELC locations of Figs. 6(a), (b), and (c), are depicted in Figs. 6(d), (e), and (f), respectively. As can be seen on the figure, a dipole mode occurs also when the ELC is located at the symmetric, as well as non-symmetric, locations near-by the face of the considered PC structure. In consequence hereof, sub-wavelength resonances also occur for such ELC locations. Although not shown inhere, the radiation resistance values at resonance decrease as the ELC moves away from the corners of the structure. Moreover, a slight shift in the outer shell radius ρ_2 value occurs in these

#113924 - $15.00 USD Received 6 Jul 2009; revised 20 Aug 2009; accepted 21 Aug 2009; published 26 Aug 2009

cases, relative to the previous case where the ELC was located at $(\rho_s, \phi_s) =$ (5.75 mm, 0°), since the resonance now occurs for $\rho_2 = 10.2887$ mm in Fig. 6 (d), for $\rho_2 = 10.288$ mm in Fig. 6 (e), and for $\rho_2 = 10.2896$ in Fig. 6 (f), as compared to $\rho_2 = 10.289$ mm for the previous case reported in Fig. 5 (g).

3.4 Loss and Dispersion

It is well-known that any realizable MNG material is dispersive and lossy [3]. In order to investigate the effects of these realistic MNG material characteristics on the sub-wavelength resonances of the PCs, the Drude and Lorentz dispersion models are employed for the permeability of the MNG shell. These models can in general be expressed as [3]

$$\mu_2(\omega) = \mu_0 \left(1 - \frac{\omega_p^2}{\omega^2 - j\Gamma\omega - \omega_r^2} \right), \tag{6}$$

where ω_p and Γ, respectively, are the magnetic plasma and collision frequencies. For the Lorentz model, the parameter ω_r is non-zero and it denotes the resonance frequency of the permeability. For the Drude model, the resonance frequency of the permeability is $\omega_r = 0$. Both dispersion models are designed to recover, at the angular frequency of operation $\omega_0 = 2\pi f_0$, with $f_0 = 300$ MHz, the value of the permeability of the lossless MNG shell, $\mu_2 = -4\mu_0$ used previously. To this end, the collision frequency $\Gamma = 10^{-3}\omega_0$ for both models, this implying that the models are slightly lossy. Moreover, the resonance frequency of the permeability of the MNG shell is set to $\omega_r = 2\pi f_r$, where $f_r = 290$ MHz.

The effects of loss and dispersion on the sub-wavelength resonances are illustrated in Fig. 7 where the radiation resistance of the n-sided PCs, $n = 48$, $n = 24$, $n = 12$, $n = 8$, and $n = 4$ (only $\rho_{f1} = 1/\sqrt{2}$ mm bend radius is shown!) in the cases where the MNG shell is described by a non-dispersive model [19] (Fig. 7 (a)), Drude dispersion model (Fig. 7 (b)), and Lorentz dispersion model (Fig. 7 (c)). The results of the canonical CC are also included, and for both CC as well as PCs, the ELC is located at $(\rho_s, \phi_s) = (5.75\text{ mm}, 0^o)$. It is clear from Fig. 7 that the resonances occur in all cases. While they are broad-band in the non-dispersive case with high values of R_r^t, they narrow considerably when dispersion is present, whereas the value of R_r^t decreases owing to the losses; this is particularly true for the Lorentz model where the losses are more severe than in the Drude model. It is moreover interesting to note that as the number of sides in the PC decreases, the radiation resistance increases. However, it is important to remark that the results for the PCs are qualitatively close to those of the CCs, this implying that it is the dispersion model rather than the geometrical shape that determines the behavior of the resonances for the investigated ELS locations.

#113924 - $15.00 USD Received 6 Jul 2009; revised 20 Aug 2009; accepted 21 Aug 2009; published 26 Aug 2009

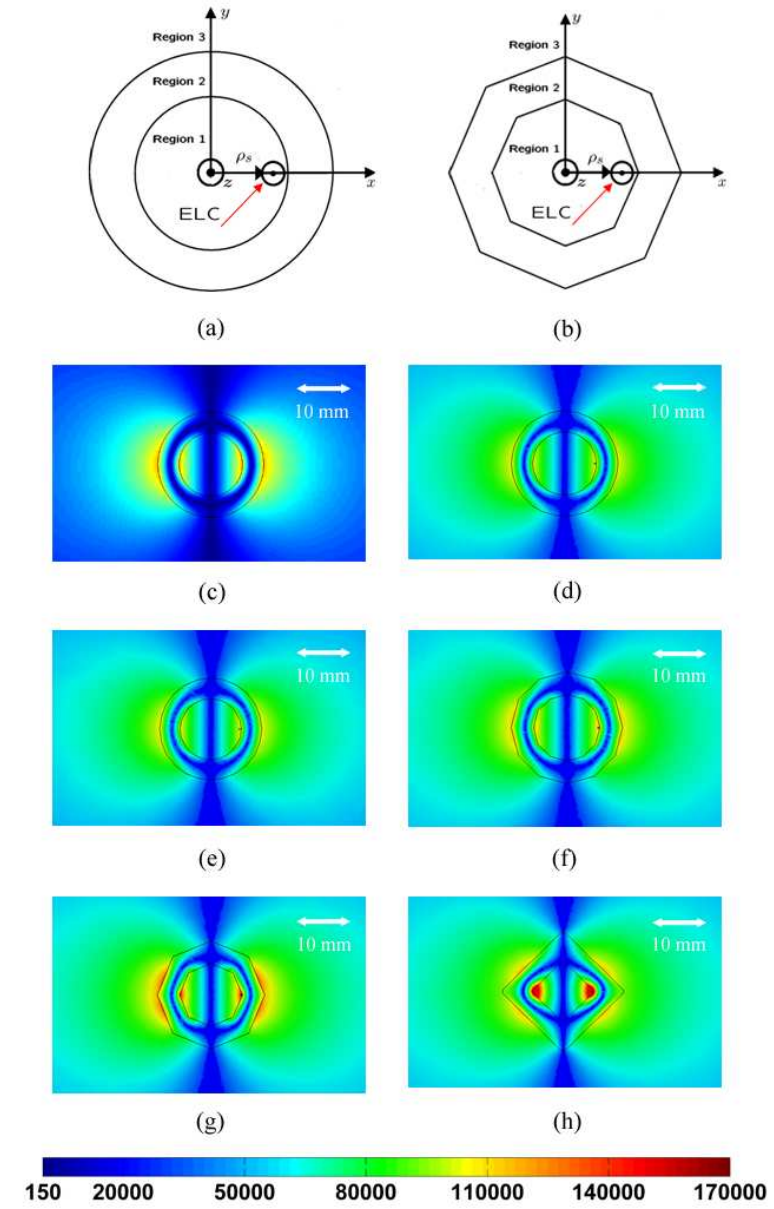

Fig. 5. The magnitude of the electric near field for the resonant CC (c) and *n*-sided PCs, with *n* = 48 (d), *n* = 24 (e), *n* = 12 (f), *n* = 8 (g) and *n* = 4 (h). In all cases, the field is depicted in the *xy*-plane and the linear dynamic range is set to [150-170000] V/m, while the ELC is located at $(\rho_s, \phi_s) = (5.75 \text{ mm}, 0^\circ)$, see also Figs. 4(a) and (b) for an indication of the ELC location. For the 4-sided PC, only the results for the 4-sided(1) PC are shown. A left-right arrow, indicating the size scale of the figure, and curves, representing the circular and polygonal surfaces of the MNG shell, are indicated in all cases.

#113924 - $15.00 USD Received 6 Jul 2009; revised 20 Aug 2009; accepted 21 Aug 2009; published 26 Aug 2009

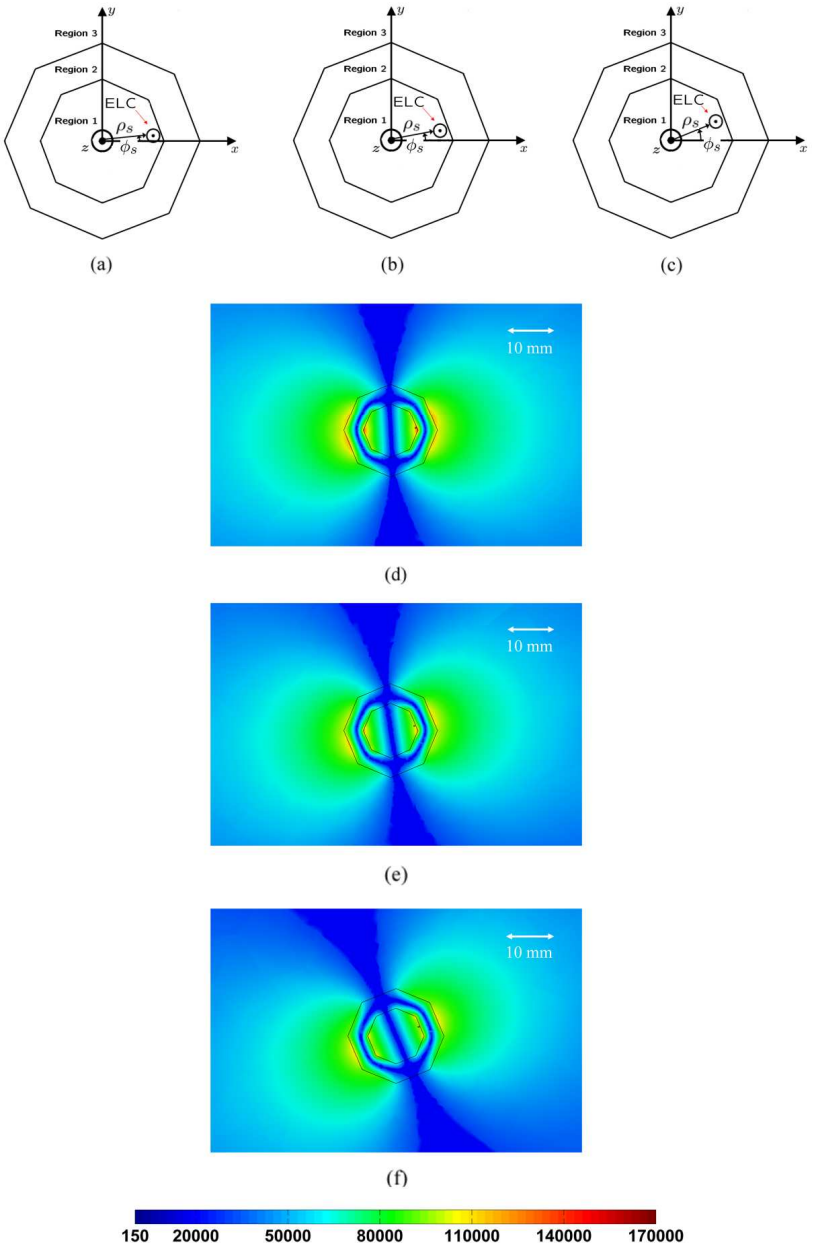

Fig. 6. The magnitude of the electric near field for the 8-sided resonant PC with the ELC located at $(\rho_s, \phi_s) =$ (5.55 mm, 5.625°) (d), $(\rho_s, \phi_s) =$ (5.32 mm, 11.25°) (e), and $(\rho_s, \phi_s) =$ (5.29 mm, 22.50°) (f), see also Figs. 6(a), (b) and (c) for an indication of the ELC location. The latter ELC location is symmetric with respect to a plane of the structure, whereas the former two are not. The field is depicted in the *xy*-plane and the linear dynamic range is set to [150-170000] V/m. A left-right arrow, indicating the size scale of the figure, and curves, representing the circular and polygonal surfaces of the MNG shell, are indicated in all cases.

#113924 - $15.00 USD Received 6 Jul 2009; revised 20 Aug 2009; accepted 21 Aug 2009; published 26 Aug 2009

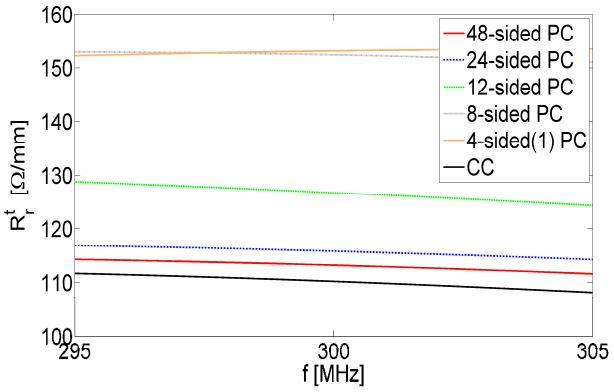

(a)

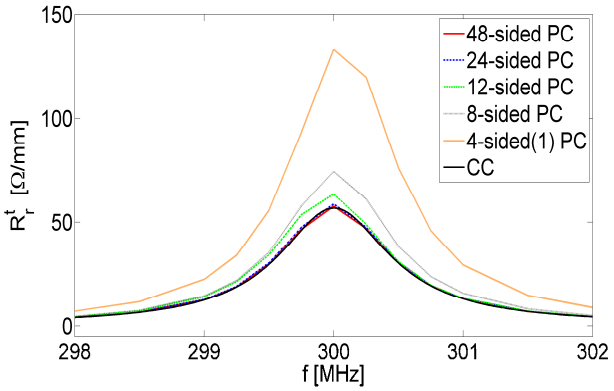

(b)

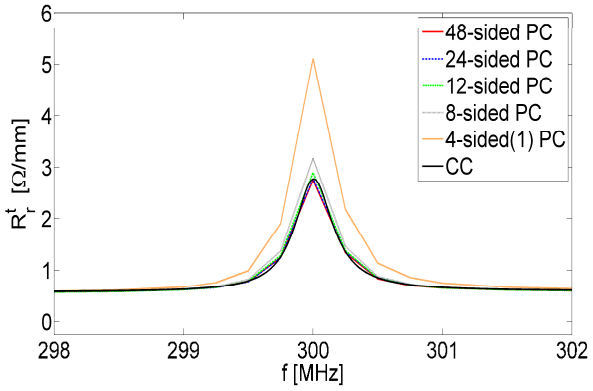

(c)

Fig. 7. Radiation resistance R_r^t [Ω / mm] as a function of frequency f for the resonant CC and n-sided PCs, where n = 48, 24, 12, 8, and 4 in the cases where the MNG shell is modeled with no dispersion (a), Drude dispersion (b), and Lorentz dispersion (c). For the 4-sided PC, only the results for the 4-sided(1) PC are shown.

#113924 - $15.00 USD Received 6 Jul 2009; revised 20 Aug 2009; accepted 21 Aug 2009; published 26 Aug 2009

4. Summary and conclusions

In this work a systematic numerical study of circular and polygonal MTM cylinders excited by a nearby ELC was conducted through a detailed investigation of their near- and far-field properties. The purpose of this study was to determine the influence of the deviation from the perfect cylindrical shape on the sub-wavelength resonances.

It was found that the sub-wavelength resonances of the circular MTM cylinders are also present in the polygonal MTM cylinders. More specifically, circular and polygonal MTM cylinders supporting dipolar mode resonances were studied, and it was demonstrated that the excitation of this mode leads to large radiation resistances. It is important to emphasize that this effect is independent of the number of polygonal sides, the location of the ELC, as well as the material dispersion model used to analyze the configurations. Hence, the sub-wavelength resonances are not limited to circularly shaped structures but they occur also for other shapes. The existence of resonances is determined mostly by the material parameters and material models and less by the geometrical shape which has an influence only on the precise values of the resonances.

Acknowledgements

This work is supported by the Danish Research Council for Technology and Production Sciences within the TopAnt project (http://topant.dtu.dk).

#113924 - $15.00 USD Received 6 Jul 2009; revised 20 Aug 2009; accepted 21 Aug 2009; published 26 Aug 2009